






Article

Optimizing the Gamma Ray-Based Detection System to Measure the Scale Thickness in Three-Phase Flow through Oil and Petrochemical Pipelines in View of Stratified Regime

Abdulilah Mohammad Mayet ¹, Tzu-Chia Chen ^{2,3,*}, Seyed Mehdi Alizadeh ⁴, Ali Awadh Al-Qahtani ¹, Abdullah K. Alanazi ⁵, Nivin A. Ghamry ⁶, Hala H. Alhashim ⁷ and Ehsan Eftekhari-Zadeh ^{8,*}

- ¹ Electrical Engineering Department, King Khalid University, Abha 61411, Saudi Arabia
² College of Management and Design, Ming Chi University of Technology, New Taipei City 243303, Taiwan
³ International College, Krirk University, 3 Ram Inthra Rd, Khwaeng Anusawari, Khet Bang Khen, Krung Thep Maha Nakhon, Bangkok 10220, Thailand
⁴ Petroleum Engineering Department, Australian University, West Mishref 13015, Kuwait
⁵ Department of Chemistry, Faculty of Science, Taif University, P.O. Box 11099, Taif 21944, Saudi Arabia
⁶ Faculty of Computers and Artificial Intelligence, Cairo University, Giza P.O. Box 12613, Egypt
⁷ Department of Physics, College of Science, Imam Abdulrahman Bin Faisal University, P.O. Box 1982, City Dammam 31441, Saudi Arabia
⁸ Institute of Optics and Quantum Electronics, Friedrich Schiller University Jena, Max-Wien-Platz 1, 07743 Jena, Germany
* Correspondence: tzuchiachen1688@gmail.com (T.-C.C.); e.eftekhari-zadeh@uni-jena.de (E.E.-Z.)



Citation: Mayet, A.M.; Chen, T.-C.; Alizadeh, S.M.; Al-Qahtani, A.A.; Alanazi, A.K.; Ghamry, N.A.; Alhashim, H.H.; Eftekhari-Zadeh, E. Optimizing the Gamma Ray-Based Detection System to Measure the Scale Thickness in Three-Phase Flow through Oil and Petrochemical Pipelines in View of Stratified Regime. *Processes* **2022**, *10*, 1866. <https://doi.org/10.3390/pr10091866>

Academic Editors: Tianshou Ma and Yuqiang Xu

Received: 15 August 2022
Accepted: 10 September 2022
Published: 15 September 2022

Publisher's Note: MDPI stays neutral with regard to jurisdictional claims in published maps and institutional affiliations.



Copyright: © 2022 by the authors. Licensee MDPI, Basel, Switzerland. This article is an open access article distributed under the terms and conditions of the Creative Commons Attribution (CC BY) license (<https://creativecommons.org/licenses/by/4.0/>).

Abstract: As the oil and petrochemical products pass through the oil pipeline, the sediment scale settles, which can cause many problems in the oil fields. Timely detection of the scale inside the pipes and taking action to solve it prevents problems such as a decrease in the efficiency of oil equipment, the wastage of energy, and the increase in repair costs. In this research, an accurate detection system of the scale thickness has been introduced, which its performance is based on the attenuation of gamma rays. The detection system consists of a dual-energy gamma source (²⁴¹Am and ¹³³Ba radioisotopes) and a sodium iodide detector. This detection system is placed on both sides of a test pipe, which is used to simulate a three-phase flow in the stratified regime. The three-phase flow includes water, gas, and oil, which have been investigated in different volume percentages. An asymmetrical scale inside the pipe, made of barium sulfate, is simulated in different thicknesses. After irradiating the gamma-ray to the test pipe and receiving the intensity of the photons by the detector, time characteristics with the names of sample SSR, sample mean, sample skewness, and sample kurtosis were extracted from the received signal, and they were introduced as the inputs of a GMDH neural network. The neural network was able to predict the scale thickness value with an RMSE of less than 0.2, which is a very low error compared to previous research. In addition, the feature extraction technique made it possible to predict the scale value with high accuracy using only one detector.

Keywords: GMDH neural network; data mining; scale thickness; stratified flow regime; oil products

1. Introduction

The presence of scale inside oil pipes causes problems such as reducing the cross-section of oil pipes, disrupting the performance of oil equipment, increasing the cost and time of repairs, and even emergency shutdown of the oil field. Using an accurate and non-invasive diagnostic system to diagnose this problem and take action to fix it can prevent the above-mentioned problems. In recent years, systems based on gamma-ray attenuation to determine the parameters of the type of flow regime and volume percentages in three-phase [1–3] and two-phase [4–6] fluids have received much attention from researchers. In these researches, different gamma sources have been investigated. Still, the big problem

of these researches is the use of two or more detectors, which has increased the cost and complexity of the detection structure. In study [7], researchers proposed a system based on gamma rays to determine volume percentages and type of flow regimes, whose detection structure consisted of a cesium source and two sodium iodide detectors. They simulated a two-phase flow in different volume percentages and three regimes of annular, stratified, and homogeneous using Monte Carlo N Particle (MCNP) code. In order to increase the accuracy, they examined several time characteristics and introduced the best time characteristic with an innovative method. The use of two detectors is the most fundamental gap of this research, which, in addition to imposing a high cost on system design, has increased the complexity of the detection system. In [8], researchers investigated the performance of the GMDH neural network, but the lack of characteristic extraction and the use of raw signals as inputs of the neural network prevented access to high accuracy. In the following research [9], the researchers put the temporal characteristics as the inputs of the GMDH neural network. This neural network has the ability to self-organize and can recognize the network structure and appropriate inputs automatically. They predicted the type of flow regimes and volume percentages with high accuracy. Alamoudi et al. [10] proposed an in-pipe scale value detection system. The proposed detection structure consisted of a dual-energy gamma source and two detectors placed opposite each other on either side of a test pipe. In the test pipe, a two-phase flow of oil and gas in different volume percentages was simulated. They did not check the characteristics of the received signals, which made not only the accuracy of their proposed system not high, but also the structure of the introduced system was complex and expensive. The use of radioisotope devices has problems such as the need to use protective clothing, difficult transportation, inability to turn off, etc.; for this reason, in recent years, the use of X-ray tubes to determine various parameters of Multiphase flows has been studied by researchers. In [11], to determine the type of flow regime and volume percentages in two-phase flows, a system consisting of an X-ray tube and a detector was introduced. They extracted temporal characteristics from the signals received by the detector and considered them as inputs of the MLP neural network. Two neural networks were designed that were responsible for determining the type of flow regimes and the percentage of void fraction separately. In [12], a three-phase flow was simulated in three different regimes and different volume percentages. The simulated structure consisted of an X-ray tube and two sodium iodide detectors. The received signals were processed in the frequency domain, and four frequency characteristics were considered as the inputs of the RBF neural network. Three RBF neural networks were trained, two of which had the task of determining volume percentages, and the other one had the task of determining the type of flow regimes. The X-ray tube has also been used to determine the type and amount of product passing through oil pipelines [13,14]. In [13], four petroleum products were simulated in a two-by-two combination in a test pipe. An X-ray tube was placed on one side of the pipe, and a sodium iodide detector was placed on the other side of the pipe directly in front of the source. The signals received from each simulation without any processing were simultaneously considered as the input of three MLP neural networks, and the volume ratio of each product was predicted with a mean absolute error of less than 2.72. In the next research [14], in order to increase the accuracy of the proposed system in research [14], the received signals were processed using wavelet transform, and the characteristics of approximate and detailed signals were extracted. They increased the accuracy of the detection system by about two times.

Inspired by previous researches, in current research, an attempt has been made to implement a system for detecting the amount of scale inside an oil pipe while a three-phase regime is passing through it. This research has tried to improve two important parameters, such as increasing accuracy and simplifying the detected system, using time characteristic extraction techniques. These are the contributions made by this study:

1. Extracting signal features by the use of statistical formulas.
2. Utilizing a single detector reduces expenses and the complexity of the detection system's structure.

3. Improving scale thickness determination accuracy by the extraction of valuable properties from received signals
4. Determining scale thickness using the GMDH neural network as a self-organizing network.

2. MCNP Simulation Setup

MCNP code has been used to simulate the detection structure. In this simulation, a dual-energy gamma source, a steel pipe, with an inner diameter of 10 cm and a thickness of 0.5 cm, and a sodium iodide detector are used. The simulated structure is shown in Figure 1. The dual-energy source consists of ^{241}Am and ^{133}Ba , are capable of emitting photons with energies of 59 and 356 KeV, respectively. In the test pipe, a three-phase flow consisting of water, oil, and gas was simulated in a stratified flow regime. Different volume percentages in the range of 10% to 80% were investigated for each phase. The considered scale was made of barium sulfate (BaSO_4) with a density of $4.5 \text{ g} \cdot \text{cm}^{-3}$. Seven different scale thicknesses, including 0, 0.05, 1, 1.5, 2, 2.5, and 3 cm, were simulated inside the pipe. The sodium iodide detector with dimensions of $2.54 \text{ cm} \times 2.54 \text{ cm}$ was placed at a distance of 30 cm and directly in front of the gamma source. 252 different simulations were performed, and all the collected data were labeled for use in the next step. The graph of the spectrum received by the detector for two scale thicknesses of 0 cm and 1.5 cm is shown in Figure 2.

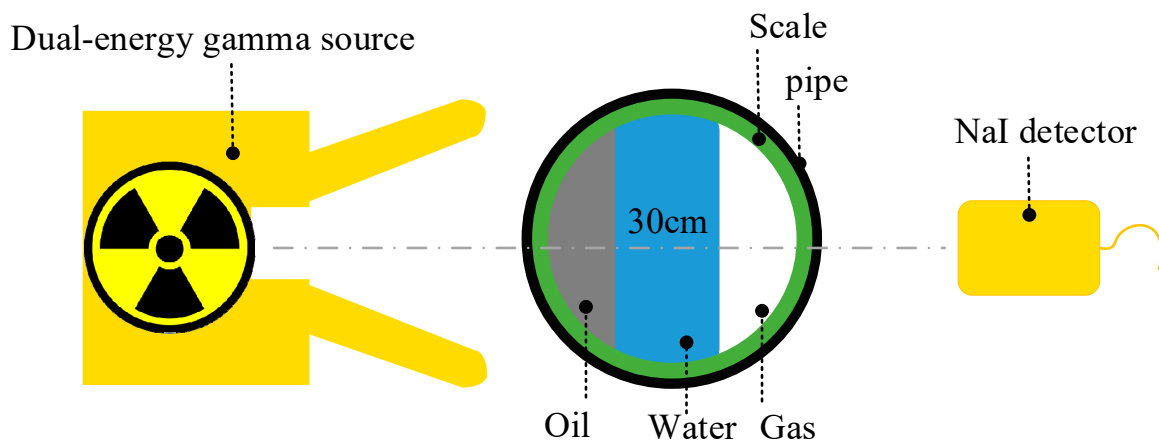


Figure 1. The structure of the simulated detection system.

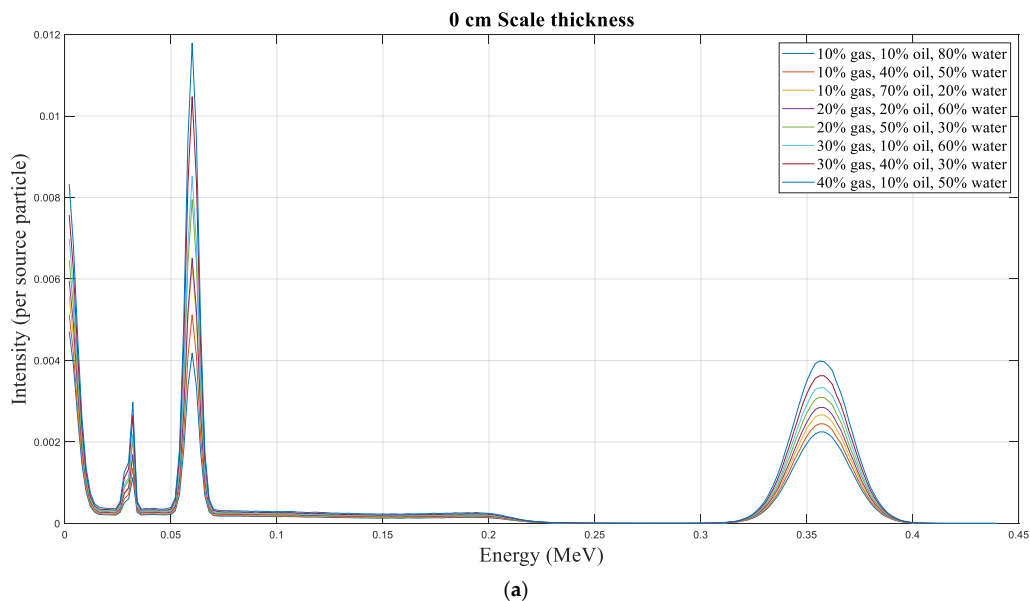


Figure 2. Cont.

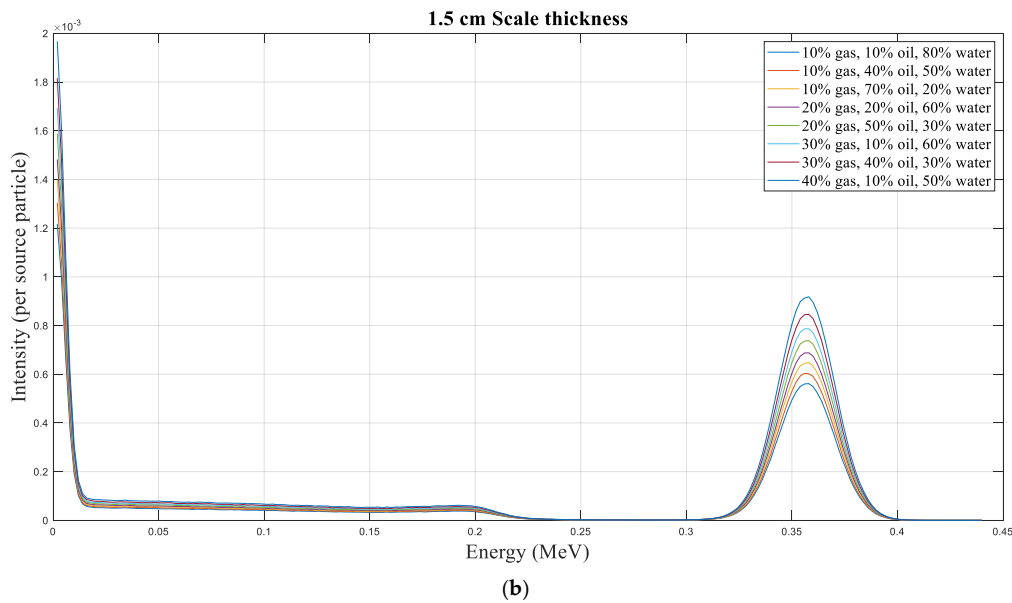


Figure 2. Spectrum received by sodium iodide detector for scale thickness of (a) 0 cm and (b) 1.5 cm.

LamberteBeer's law is used to determine the attenuation rate when a narrow gamma ray strikes an object.

$$I = I_0 e^{-\mu \rho x} \quad (1)$$

I , I_0 , μ and ρ denote the intensity of un-collided, the original photons, the mass attenuation coefficient, and the material density of the absorber, respectively. X denotes how far the beam travels through the absorber. Equation (1) states that different objects respond to gamma radiation in different ways. This variation in behavior determines the kind and amount of a substance in the environment. A $2.54 \text{ cm} \times 2.54 \text{ cm}$ NaI detector was used in this research to capture the photons that were transmitted. The detector was used to record photon energy spectra using pulse height tally (Tally F8). Previous analyses have supported the study's reproductive outcomes [6]. Several research laboratory structures were used in this review, and the results from the MCNP code were compared with them. Both were normalized to units to examine exploratory and reenactment data because the Tally output in the MCNP procedure is per source particle. The disparity between the simulation results and the lab setup represented the largest relative error at 2.2%.

3. Time-Domain Feature Extraction

The signals collected in the previous section had many dimensions, and their interpretation was a very complicated and time-consuming task. For this purpose, to simplify and separate the available data, an attempt was made to extract time characteristics. Four time-characteristics with the names of sample mean, sample of summation of square root (SSR), sample skewness, and sample kurtosis were extracted from the signals recorded by the NaI detector. These features have been used to improve the accuracy and structure of the scale thickness detection system since they were first introduced as helpful characteristics in earlier study [7,9,11]. The equations of these features are given below:

- Sample mean:

$$m = \frac{1}{N} \sum_{n=1}^N x(n) \quad (2)$$

- Sample of summation of square root (SSR):

$$SSR = \sum_{n=1}^N (x(n))^{0.5} \quad (3)$$

- Sample skewness:

$$Skewness = \frac{m_3}{\sigma^3}, m_3 = \frac{1}{N} \sum_{n=1}^N [x(n) - m]^3 \tag{4}$$

- Sample kurtosis:

$$Kurtosis = \frac{m_4}{\sigma^4}, m_4 = \frac{1}{N} \sum_{n=1}^N [x(n) - m]^4 \tag{5}$$

Here n is the dataset’s values, N denotes the total data number, and $x(n)$ represents the principal signal in the time domain.

The diagram of these four characteristics in terms of volume percentage of gas and oil is shown in Figure 3. As it is clear from this figure, the amount of scale thickness can be separated into different volume percentages. These characteristics have been used to train the GMDH neural network. As mentioned in the previous section, 252 different simulations have been performed, and four time characteristics have been extracted from the signal received from each simulation. Therefore, the available matrix contains 4 rows and 252 columns. The output of the neural network is also the value of the thickness of the scale inside the pipe in centimeters.

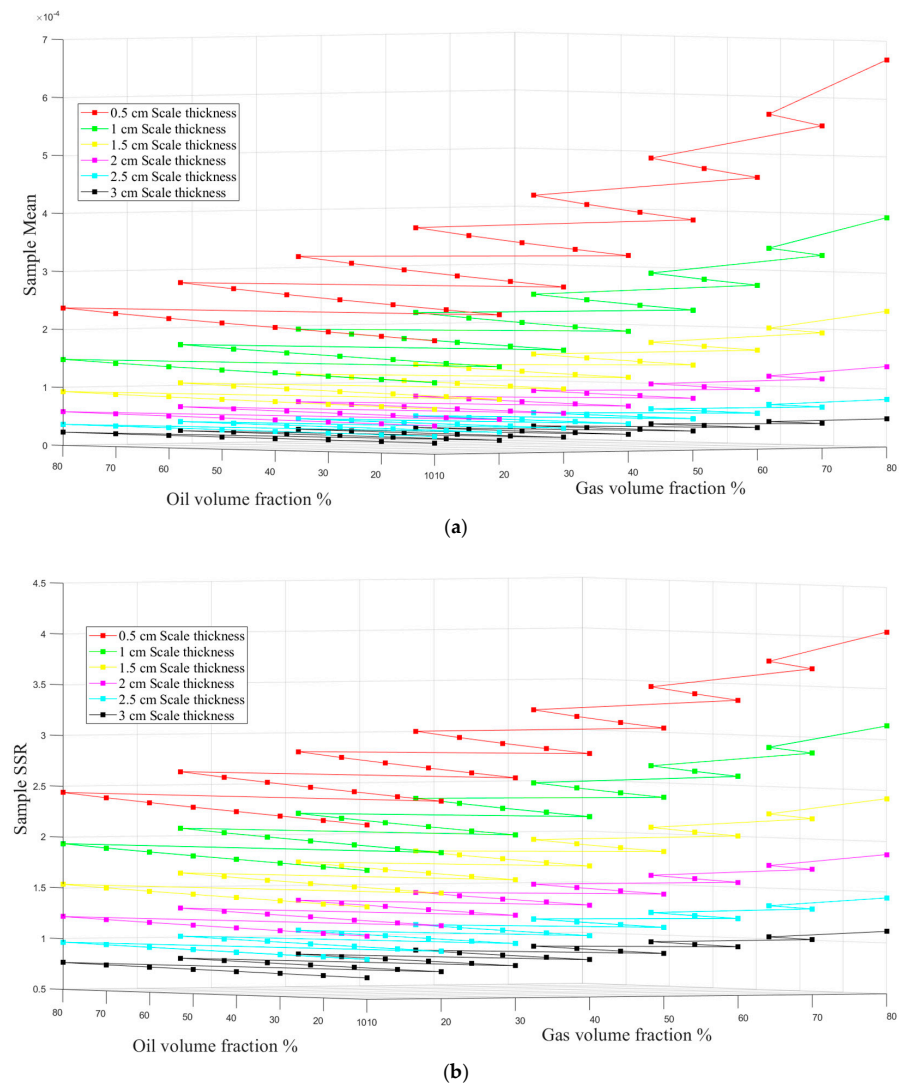


Figure 3. Cont.

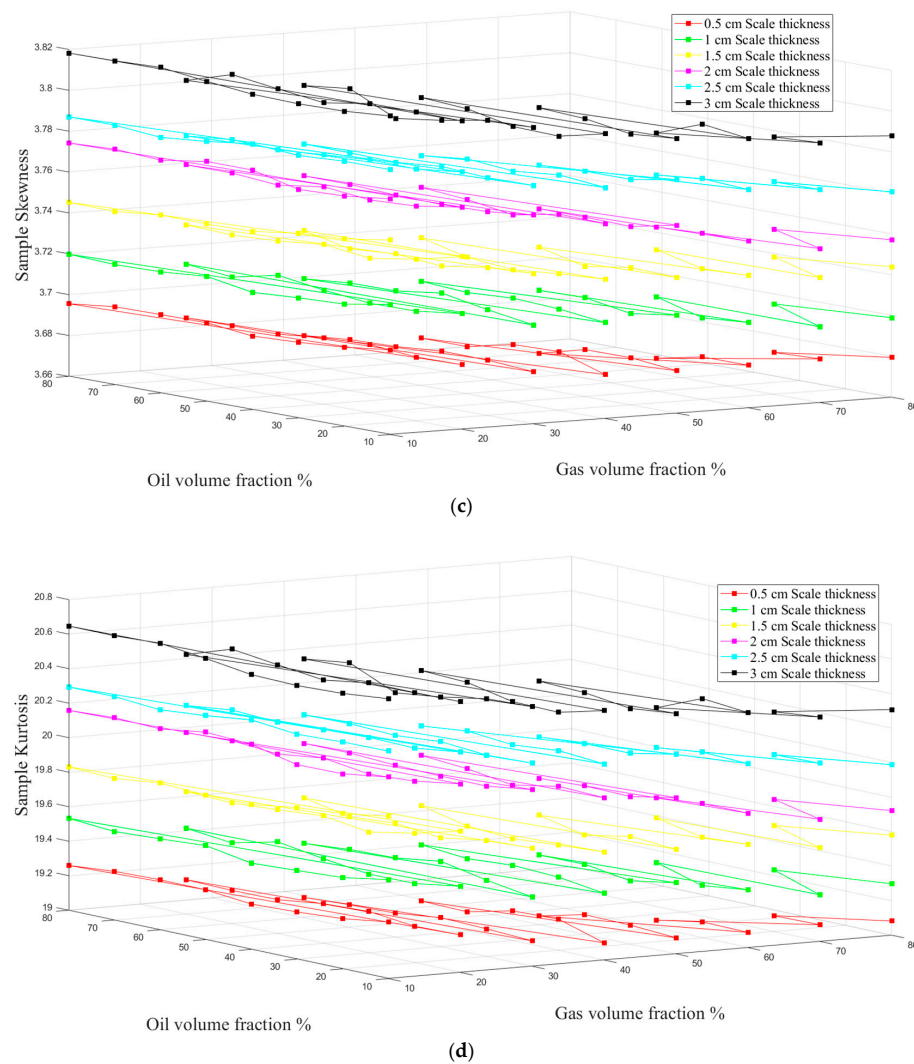


Figure 3. Extracted temporal characteristics in terms of volume percentage of gas and oil (a) sample mean, (b) sample SSR, (c) sample skewness, and (d) sample kurtosis.

4. GMDH Neural Network

In 1968, a Ukrainian mathematician named M.G. Ivakhnenko presented a mathematical model to solve prediction and classification problems and called it Group Method of Data Handling (GMDH) [15]. The model proposed by Ivakhnenko has self-organization capability so that the network structure, effective inputs, number of hidden layers, and number of neurons of hidden layers are automatically selected. In this neural network, the relationship between input and output is described by the Kolmogorov-Gabor polynomial, which is described below.

$$y = a_0 + \sum_{i=1}^m a_i x_i + \sum_{i=1}^m \sum_{j=1}^m a_{ij} x_i x_j + \sum_{i=1}^m \sum_{j=1}^m \sum_{k=1}^m a_{ijk} x_i x_j x_k + \dots \quad (6)$$

where a (a_1, a_2, \dots, a_m) are weights or coefficients of vector, X (x_1, x_2, \dots, x_m) are also vector inputs or the same extracted features, and y is the output of the network. GMDH neural network is implemented in 5 steps, which are as follows.

1. All neural network inputs (extracted characteristics) two at the time and for each $\binom{m}{2}$ admixture are fitted to the quadratic polynomial given in Equation (7). The purpose of this step is to calculate the C coefficients that are obtained with the least

squares algorithm. The output of each quadratic polynomial predicts the desired output value. The task of calculating these polynomials is assigned to the neurons of the neural network.

$$Z = c_1 + c_2x_i + c_3x_j + c_4x_i^2 + c_5x_j^2 + c_6x_ix_j \quad (7)$$

2. The neurons with the most error in predicting the desired output are removed.
3. The neurons selected in the previous step are considered quadratic polynomial inputs described in step one. In this step, polynomials are produced from polynomials, producing a polynomial with a higher order.
4. The second step is repeated, and neurons with high errors are removed. This repetition of the steps and generation of polynomials from polynomials are repeated until the desired error value is obtained.
5. Checking network performance with test data. In the design of neural networks, the major of the data (about 70%) are used for training the neural network, and the rest of the data are used for the final test of the network. The correct performance of the neural network against these data sets ensures that the designed network can show acceptable performance in operational conditions. In order to identify various characteristics in many scientific domains, several studies have employed intelligent computer systems [16–37].

5. Results

A GMDH neural network with four inputs and one output was trained. The inputs of this network were the extracted temporal characteristics, and the network's output was the value of the scale thickness inside the pipe in centimeters. 252 samples were available for the implementation of this network, of which 176 samples were assigned to the training data, and the remaining samples were used for the final test of the neural network. The selection of these samples was done randomly so that the neural network could be trained with all the range of data. According to the self-organizing capability of the GMDH neural network, the structure that had the best accuracy is shown in Figure 4. This network has 3 hidden layers, and the number of selected neurons in these layers was 4, 4, and 2, respectively. A regression diagram and error diagram have been used to show the performance of the designed neural network. In the regression diagram, the yellow line shows the desired output, and the green circles represent the output of the neural network. The closer the yellow line and the green circle are to each other, the more accurate the designed neural network is. The error diagram shows the difference between the network output and the desired output for each sample. The regression and error graphs for the training and testing datasets are shown in Figure 5. In order to obtain the error value, two widely used criteria named Mean Square Error (MSE) and Root Mean Square Error (RMSE) were calculated with the following equations:

$$MSE = \frac{\sum_{j=1}^N (X_j(Exp) - X_j(Pred))^2}{N} \quad (8)$$

$$RMSE = \left[\frac{\sum_{j=1}^N (X_j(Exp) - X_j(Pred))^2}{N} \right]^{0.5} \quad (9)$$

In which N indicates data number, 'X (Exp)', and 'X (Pred)' illustrate the experimental and predicted (ANN) values, respectively.

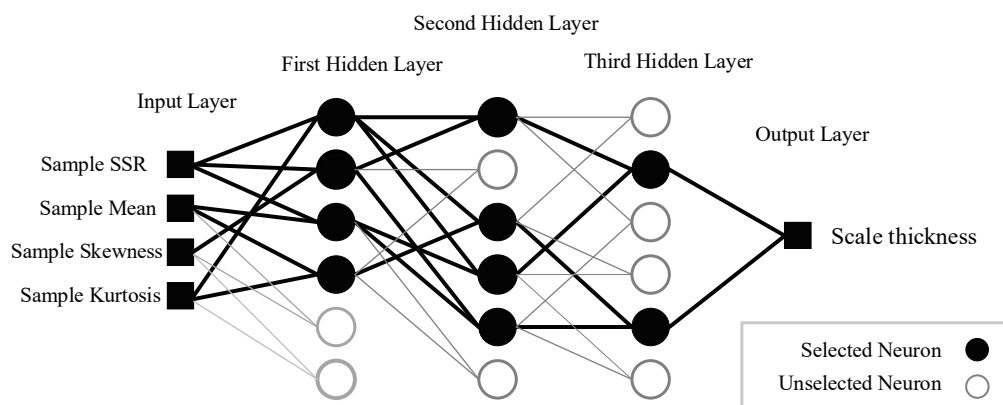


Figure 4. The structure of the trained GMDH neural network.

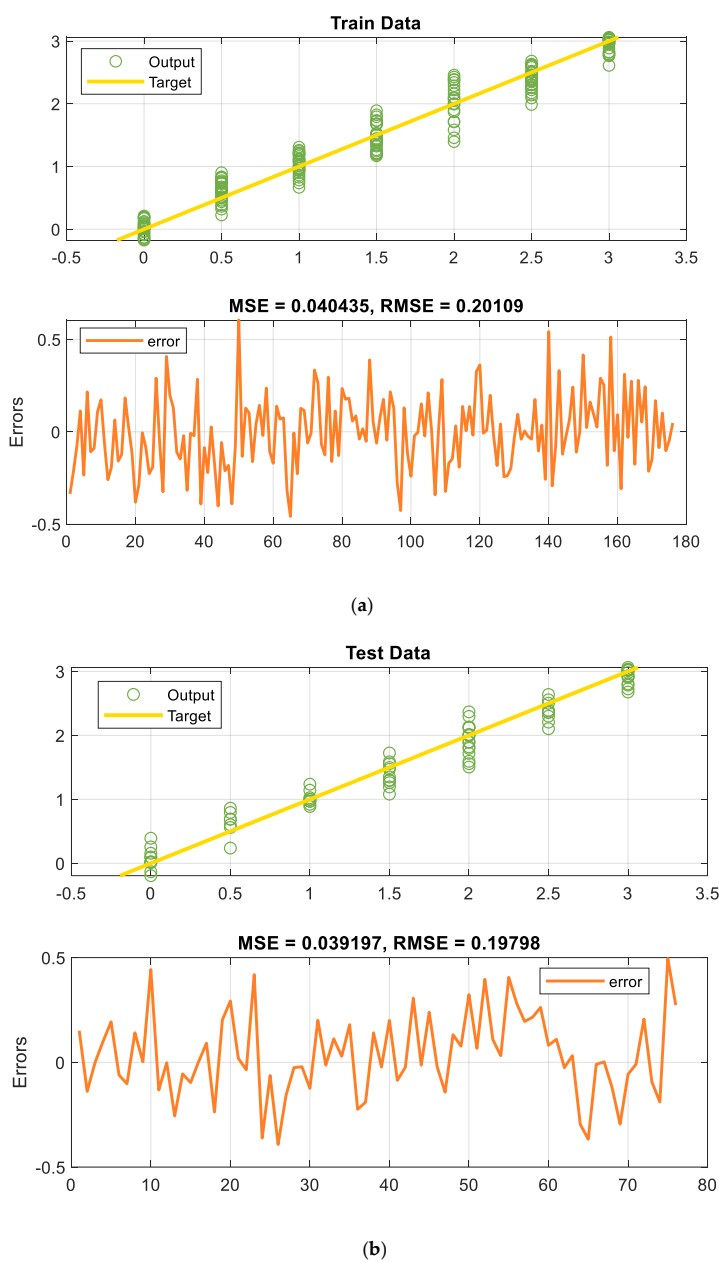


Figure 5. Performance of designed GMDH neural network against (a) training and (b) testing data.

The comparison table of the output of the neural network with the desired output is given in Table 1. To show the accuracy of the implemented system, Table 2 shows a comparison between the accuracy of current research and previous research. Extracting the appropriate features from the received signals has not only improved the accuracy of the presented system, but also reduced the number of detectors. Reducing the number of detectors, along with reducing the complexity of the system, will significantly reduce the implementation cost of the detection system.

Table 1. Comparison of target values with neural network outputs.

<i>Data Number</i>	<i>Train Targets</i>	<i>Train Outputs</i>	<i>Test Targets</i>	<i>Test Outputs</i>
1	0.5000	0.8364	1.5000	1.3493
2	1.0000	1.2139	2.5000	2.6387
3	1.0000	1.0764	1.0000	0.9995
4	3.0000	2.8872	2.0000	1.8995
5	1.5000	1.7345	0	−0.1932
6	1.0000	0.7840	0.5000	0.5605
7	0	0.1079	0.5000	0.6024
8	0	0.0893	2.5000	2.3590
9	2.5000	2.3907	2.0000	1.9970
10	1.0000	0.8268	2.0000	1.5573
11	0	0.0608	2.0000	2.1318
12	1.0000	1.2595	2.5000	2.5019
13	1.0000	1.1938	0	0.2556
14	2.5000	2.4362	2.5000	2.5553
15	0.5000	0.6588	0	0.0966
16	2.5000	2.6227	1.5000	1.4977
17	3.0000	2.8169	3.0000	2.9088
18	3.0000	2.9739	1.0000	1.2369
19	2.5000	2.6138	2.0000	1.7970
20	2.0000	2.3813	2.5000	2.2073
21	2.0000	2.2872	3.0000	2.9807
22	0	0.0054	3.0000	3.0354
23	0.5000	0.5838	1.5000	1.0813
24	1.5000	1.7266	0.5000	0.8614
25	0	0.1918	3.0000	3.0631
26	2.0000	1.7102	0	0.3922
27	0	0.0498	0	0.1574
28	1.5000	1.8249	1.0000	1.0251
29	2.5000	2.0919	0	0.0212
30	2.5000	2.3027	2.0000	2.1242
31	0	−0.1304	2.5000	2.2996
32	2.5000	2.6107	3.0000	3.0133
33	0.5000	0.6473	1.0000	0.8878
34	3.0000	3.0209	1.0000	0.9709
35	0.5000	0.8172	2.0000	1.8204
36	0	0.0083	1.5000	1.7240
37	0.5000	0.5213	0.5000	0.6903
38	1.5000	1.2158	2.5000	2.3593
39	1.5000	1.8909	0	0.0223
40	2.0000	2.0860	1.5000	1.3002
41	2.0000	2.2205	1.5000	1.5859
42	1.0000	0.9735	3.0000	3.0234
43	0	0.1812	1.5000	1.1938

Table 1. Cont.

<i>Data Number</i>	<i>Train Targets</i>	<i>Train Outputs</i>	<i>Test Targets</i>	<i>Test Outputs</i>
44	0.5000	0.9019	2.0000	2.0133
45	2.0000	2.0582	1.5000	1.2607
46	0	0.2109	3.0000	3.0214
47	1.5000	1.6819	1.0000	1.1423
48	2.0000	2.3901	0	−0.1317
49	0	0.0807	1.0000	0.9227
50	2.0000	1.3950	3.0000	2.6769
51	2.5000	2.6330	3.0000	2.9334
52	2.5000	2.3719	2.5000	2.1041
53	1.5000	1.3983	2.0000	1.8912
54	1.0000	1.1618	1.5000	1.4685
55	0.5000	0.4591	2.0000	1.5945
56	2.5000	2.3568	2.0000	1.7184
57	2.5000	2.5199	3.0000	2.8049
58	3.0000	2.7633	3.0000	2.7848
59	1.0000	1.1078	0.5000	0.2380
60	0	0.1705	3.0000	2.9187
61	1.0000	0.8614	2.5000	2.3903
62	1.0000	0.9309	3.0000	3.0254
63	1.5000	1.4250	1.0000	0.9684
64	0.5000	0.8160	2.0000	2.2965
65	2.0000	2.4583	2.0000	2.3671
66	0.5000	0.5069	0	0.0096
67	0.5000	0.7269	1.0000	0.9977
68	2.5000	2.3730	2.0000	2.1213
69	1.5000	1.3851	0.5000	0.7948
70	3.0000	3.0613	1.5000	1.5571
71	1.0000	1.0067	2.0000	2.0093
72	1.0000	0.6657	1.5000	1.2935
73	1.0000	0.7362	0	0.0936
74	1.0000	1.0683	0.5000	0.6893
75	0	0.1252	2.0000	1.5044
76	1.5000	1.2048	3.0000	2.7268
77	2.0000	2.1610	-	-
78	0.5000	0.3873	-	-
79	0.5000	0.6288	-	-
80	1.5000	1.2658	-	-
81	1.5000	1.3239	-	-
82	0.5000	0.3186	-	-
83	1.0000	0.9420	-	-
84	1.5000	1.4139	-	-
85	3.0000	3.0394	-	-
86	3.0000	2.9834	-	-
87	0	0.0517	-	-
88	3.0000	2.6107	-	-
89	1.0000	0.9446	-	-
90	0.5000	0.5613	-	-
91	0	−0.0763	-	-
92	0	−0.1754	-	-
93	3.0000	3.0456	-	-
94	3.0000	2.7840	-	-
95	2.5000	2.3713	-	-

Table 1. Cont.

<i>Data Number</i>	<i>Train Targets</i>	<i>Train Outputs</i>	<i>Test Targets</i>	<i>Test Outputs</i>
96	0.5000	0.7758	-	-
97	2.0000	2.4267	-	-
98	2.0000	1.8703	-	-
99	1.0000	1.1189	-	-
100	1.0000	1.2409	-	-
101	1.0000	1.0213	-	-
102	2.0000	2.0038	-	-
103	0	-0.1516	-	-
104	1.5000	1.5227	-	-
105	3.0000	2.7891	-	-
106	1.5000	1.4973	-	-
107	2.0000	2.3414	-	-
108	3.0000	2.9899	-	-
109	2.0000	1.7173	-	-
110	0.5000	0.8231	-	-
111	1.5000	1.6692	-	-
112	0.5000	0.6473	-	-
113	0	-0.0318	-	-
114	1.0000	1.1917	-	-
115	0.5000	0.3629	-	-
116	0.5000	0.4943	-	-
117	0	-0.1362	-	-
118	3.0000	3.0185	-	-
119	2.5000	2.1735	-	-
120	2.5000	2.1380	-	-
121	0	0.0072	-	-
122	2.0000	1.9919	-	-
123	2.5000	2.3027	-	-
124	0	0.0226	-	-
125	1.5000	1.6830	-	-
126	0	-0.0423	-	-
127	0.5000	0.7433	-	-
128	0.5000	0.7383	-	-
129	0	0.1972	-	-
130	3.0000	3.0329	-	-
131	2.5000	2.4056	-	-
132	3.0000	3.0404	-	-
133	2.5000	2.4958	-	-
134	3.0000	3.0254	-	-
135	0	0.0398	-	-
136	3.0000	2.8249	-	-
137	2.5000	2.6042	-	-
138	2.5000	2.4641	-	-
139	0.5000	0.7573	-	-
140	2.0000	1.4576	-	-
141	1.5000	1.7930	-	-
142	2.5000	2.5810	-	-
143	1.5000	1.1687	-	-
144	1.0000	1.1215	-	-
145	3.0000	3.0252	-	-
146	0.5000	0.4367	-	-
147	2.5000	2.2581	-	-
148	0.5000	0.6105	-	-

Table 1. Cont.

Data Number	Train Targets	Train Outputs	Test Targets	Test Outputs
149	2.5000	2.5026	-	-
150	2.0000	1.5837	-	-
151	3.0000	2.9770	-	-
152	1.5000	1.3390	-	-
153	2.0000	1.9029	-	-
154	1.0000	0.9743	-	-
155	1.5000	1.2099	-	-
156	1.5000	1.2457	-	-
157	2.5000	2.6815	-	-
158	2.5000	1.9872	-	-
159	2.0000	2.1030	-	-
160	0	-0.0921	-	-
161	1.0000	1.3085	-	-
162	1.5000	1.1887	-	-
163	1.5000	1.5302	-	-
164	0.5000	0.2263	-	-
165	0.5000	0.6759	-	-
166	2.5000	2.2218	-	-
167	1.5000	1.4478	-	-
168	2.5000	2.2561	-	-
169	1.0000	1.2136	-	-
170	0.5000	0.6492	-	-
171	0	-0.1685	-	-
172	1.0000	1.0860	-	-
173	1.0000	0.8985	-	-
174	0.5000	0.6025	-	-
175	3.0000	3.0462	-	-
176	3.0000	2.9525	-	-

Table 2. A comparison of the accuracy of the proposed detection system and previous studies.

Ref	Number of Detectors	Source Type	Type of Neural Network	Maximum MSE	Maximum RMSE
[9]	1	^{137}Cs	GMDH	1.24	1.11
[7]	2	^{137}Cs	MLP	0.21	0.46
[8]	1	^{60}Co	GMDH	7.34	2.71
[38]	2	^{137}Cs	MLP	0.67	0.82
[39]	1	X-Ray tube	MLP	17.05	4.13
[40]	1	^{137}Cs	MLP	2.56	1.6
[41]	1	^{60}Co	RBF	37.45	6.12
[42]	2	^{137}Cs	MLP	1.08	1.04
[current study]	1	Dual-energy gamma source	GMDH	0.04	0.2

6. Conclusions

The presence of scale inside the oil pipes will cause significant problems such as reducing the effective diameter of the oil pipes, increasing the energy consumed by the oil pumps, reducing the efficiency, and increasing the repair costs. Therefore, timely detection of the amount of scale inside the oil pipes helps to reduce the mentioned damages. In this research, a non-invasive system based on gamma-ray attenuation was introduced. The introduced system consisted of a dual-energy source of ^{241}Am and ^{133}Ba , a NaI detector, and a steel pipe. A three-phase flow was simulated in a stratified regime consisting of oil, water, and gas in different volume percentages. In all these simulations, the value of different scales in the range of 0 to 3 cm were examined. All these structures and flows

passing through the test pipe were simulated by MCNP code. After collecting the received signals from the detector, the feature extraction operation started in the time domain, and four time features with the names of sample mean, sample SSR, sample skewness, and sample kurtosis were extracted from the signals and introduced as the inputs of the GMDH neural network. The trained neural network predicted the thickness of the scale inside the pipe with an RMSE of less than 0.2, which is a very low error compared to previous studies. In addition, the use of feature extraction techniques made it unnecessary to have multiple detectors, and only one detector is enough to determine the thickness of the scale, which has significantly saved the implementation costs. One of the major limitations of this research is that working with radioisotope devices requires the use of protective clothing, and the transportation of these devices is challenging. The use of feature extraction techniques in the frequency domain, time-frequency domain, and the investigation of the performance of other neural networks such as MLP, RBF, and even deep neural networks are highly recommended to the researchers in this field.

Author Contributions: Conceptualization, A.M.M. and T.-C.C.; methodology, S.M.A.; software, T.-C.C. and S.M.A.; validation, A.A.A.-Q., A.K.A. and N.A.G.; formal analysis, A.A.A.-Q.; investigation, N.A.G.; resources, A.K.A.; data curation, H.H.A.; writing—original draft preparation, H.H.A.; writing—review and editing, T.-C.C. and E.E.-Z.; visualization, E.E.-Z.; supervision, A.M.M., T.-C.C. and E.E.-Z.; project administration, A.M.M.; funding acquisition, A.M.M. and E.E.-Z. All authors have read and agreed to the published version of the manuscript.

Funding: This work was supported by the Deanship of Scientific Research at King Khalid University (Grant numbers RGP.1/243/42). The authors acknowledge support from the German Research Foundation and the Open Access Publication Fund of the Thueringer Universitaets-und Landesbibliothek Jena Projekt-Nr. 433052568; the BMBF-Projekt 05P21SJFA2 Verbundprojekt 05P2021 (ErUM-FSP T05).

Institutional Review Board Statement: Not applicable.

Informed Consent Statement: Not applicable.

Data Availability Statement: Not applicable.

Conflicts of Interest: The authors declare no conflict of interest.

References

1. Roshani, G.H.; Karami, A.; Nazemi, E.; Shama, F. Volume fraction determination of the annular three-phase flow of gas-oil-water using adaptive neuro-fuzzy inference system. *Comput. Appl. Math.* **2018**, *37*, 4321–4341. [\[CrossRef\]](#)
2. Roshani, M.; Phan, G.; Roshani, G.H.; Hanus, R.; Nazemi, B.; Corniani, E.; Nazemi, E. Combination of X-ray tube and GMDH neural network as a nondestructive and potential technique for measuring characteristics of gas-oil–water three phase flows. *Measurement* **2021**, *168*, 108427. [\[CrossRef\]](#)
3. Roshani, G.H.; Karami, A.; Nazemi, E. An intelligent integrated approach of Jaya optimization algorithm and neuro-fuzzy network to model the stratified three-phase flow of gas–oil–water. *Comput. Appl. Math.* **2019**, *38*, 1–26. [\[CrossRef\]](#)
4. Hosseini, S.; Taylan, O.; Abusurrah, M.; Akilan, T.; Nazemi, E.; Eftekhari-Zadeh, E.; Roshani, G.H. Application of Wavelet Feature Extraction and Artificial Neural Networks for Improving the Performance of Gas–Liquid Two-Phase Flow Meters Used in Oil and Petrochemical Industries. *Polymers* **2021**, *13*, 3647. [\[CrossRef\]](#)
5. Sattari, M.A.; Korani, N.; Hanus, R.; Roshani, G.H.; Nazemi, E. Improving the performance of gamma radiation based two phase flow meters using optimal time characteristics of the detector output signal extraction. *J. Nucl. Sci. Technol.* **2020**, *41*, 42–54.
6. Nazemi, E.; Roshani, G.H.; Feghhi, S.A.H.; Setayeshi, S.; Zadeh, E.E.; Fatehi, A. Optimization of a method for identifying the flow regime and measuring void fraction in a broad beam gamma-ray attenuation technique. *Int. J. Hydrog. Energy* **2016**, *41*, 7438–7444. [\[CrossRef\]](#)
7. Sattari, M.A.; Roshani, G.H.; Hanus, R.; Nazemi, E. Applicability of time-domain feature extraction methods and artificial intelligence in two-phase flow meters based on gamma-ray absorption technique. *Measurement* **2021**, *168*, 108474. [\[CrossRef\]](#)
8. Roshani, M.; Sattari, M.A.; Ali, P.J.M.; Roshani, G.H.; Nazemi, B.; Corniani, E.; Nazemi, E. Application of GMDH neural network technique to improve measuring precision of a simplified photon attenuation based two-phase flowmeter. *Flow Meas. Instrum.* **2020**, *75*, 101804. [\[CrossRef\]](#)
9. Sattari, M.A.; Roshani, G.H.; Hanus, R. Improving the structure of two-phase flow meter using feature extraction and GMDH neural network. *Radiat. Phys. Chem.* **2020**, *171*, 108725. [\[CrossRef\]](#)

10. Alamoudi, M.; Sattari, M.A.; Balubaid, M.; Eftekhari-Zadeh, E.; Nazemi, E.; Taylan, O.; Kalmoun, E.M. Application of Gamma Attenuation Technique and Artificial Intelligence to Detect Scale Thickness in Pipelines in Which Two-Phase Flows with Different Flow Regimes and Void Fractions Exist. *Symmetry* **2021**, *13*, 1198. [[CrossRef](#)]
11. Basahel, A.; Sattari, M.A.; Taylan, O.; Nazemi, E. Application of Feature Extraction and Artificial Intelligence Techniques for Increasing the Accuracy of X-ray Radiation Based Two Phase Flow Meter. *Mathematics* **2021**, *9*, 1227. [[CrossRef](#)]
12. Taylan, O.; Sattari, M.A.; Essoussi, I.E.; Nazemi, E. Frequency Domain Feature Extraction Investigation to Increase the Accuracy of an Intelligent Nondestructive System for Volume Fraction and Regime Determination of Gas–Water–Oil Three-Phase Flows. *Mathematics* **2021**, *9*, 2091. [[CrossRef](#)]
13. Roshani, G.H.; Ali, P.J.M.; Mohammed, S.; Hanus, R.; Abdulkareem, L.; Alanezi, A.A.; Kalmoun, E.M. Simulation Study of Utilizing X-ray Tube in Monitoring Systems of Liquid Petroleum Products. *Processes* **2021**, *9*, 828. [[CrossRef](#)]
14. Balubaid, M.; Sattari, M.A.; Taylan, O.; Bakhsh, A.A.; Nazemi, E. Applications of discrete wavelet transform for feature extraction to increase the accuracy of monitoring systems of liquid petroleum products. *Mathematics* **2021**, *9*, 3215. [[CrossRef](#)]
15. Ivakhnenko, A.G. Polynomial theory of complex systems. *IEEE Trans. Syst. Man Cybern.* **1971**, SMC-1, 364–378. [[CrossRef](#)]
16. Lalbakhsh, A.; Mohamadpour, G.; Roshani, S.; Ami, M.; Roshani, S.; Sayem, A.S.; Alibakhshikenari, M.; Koziel, S. Design of a compact planar transmission line for miniaturized rat-race coupler with harmonics suppression. *IEEE Access* **2021**, *9*, 129207–129217. [[CrossRef](#)]
17. Hookari, M.; Roshani, S.; Roshani, S. High-efficiency balanced power amplifier using miniaturized harmonics suppressed cou-pler. *Int. J. RF Microw. Comput. Aided Eng.* **2020**, *30*, e22252. [[CrossRef](#)]
18. Lotfi, S.; Roshani, S.; Roshani, S.; Gilan, M.S. Wilkinson power divider with band-pass filtering response and harmonics suppression using open and short stubs. *Frequenz* **2020**, *74*, 169–176. [[CrossRef](#)]
19. Jamshidi, M.; Siahkamari, H.; Roshani, S.; Roshani, S. A compact Gysel power divider design using U-shaped and T-shaped resonators with harmonics suppression. *Electromagnetics* **2019**, *39*, 491–504. [[CrossRef](#)]
20. Roshani, S.; Jamshidi, M.B.; Mohebi, F.; Roshani, S. Design and modeling of a compact power divider with squared resonators using artificial intelligence. *Wirel. Pers. Commun.* **2021**, *117*, 2085–2096. [[CrossRef](#)]
21. Roshani, S.; Azizian, J.; Roshani, S.; Jamshidi, M.B.; Parandin, F. Design of a miniaturized branch line microstrip coupler with a simple structure using artificial neural network. *Frequenz* **2022**, *76*. [[CrossRef](#)]
22. Khaleghi, M.; Salimi, J.; Farhangi, V.; Moradi, M.J.; Karakouzian, M. Application of Artificial Neural Network to Predict Load Bearing Capacity and Stiffness of Perforated Masonry Walls. *CivilEng* **2021**, *2*, 48–67. [[CrossRef](#)]
23. Dabiri, H.; Farhangi, V.; Moradi, M.J.; Zadehmohamad, M.; Karakouzian, M. Applications of Decision Tree and Random Forest as Tree-Based Machine Learning Techniques for Analyzing the Ultimate Strain of Spliced and Non-Spliced Reinforcement Bars. *Appl. Sci.* **2022**, *12*, 4851. [[CrossRef](#)]
24. Zych, M.; Petryka, L.; Kępczyński, J.; Hanus, R.; Bujak, T.; Puskarczyk, E. Radioisotope investigations of compound two-phase flows in an open channel. *Flow Meas. Instrum.* **2014**, *35*, 11–15. [[CrossRef](#)]
25. Zych, M.; Hanus, R.; Wilk, B.; Petryka, L.; Świsulski, D. Comparison of noise reduction methods in radiometric correlation measurements of two-phase liquid-gas flows. *Measurement* **2018**, *129*, 288–295. [[CrossRef](#)]
26. Golijanek-Jędrzejczyk, A.; Mrowiec, A.; Hanus, R.; Zych, M.; Heronimczak, M.; Świsulski, D. Uncertainty of mass flow measurement using centric and eccentric orifice for Reynolds number in the range $10,000 \leq Re \leq 20,000$. *Measurement* **2020**, *160*, 107851. [[CrossRef](#)]
27. Mayet, A.; Hussain, M. Amorphous W_Nx Metal For Accelerometers and Gyroscope. In Proceedings of the MRS Fall Meeting, Boston, MA, USA, 30 November–5 December 2014.
28. Mayet, A.; Hussain, A.; Hussain, M. Three-terminal nanoelectromechanical switch based on tungsten nitride—An amorphous metallic material. *Nanotechnology* **2016**, *27*, 035202. [[CrossRef](#)]
29. Shukla, N.K.; Mayet, A.M.; Vats, A.; Aggarwal, M.; Raja, R.K.; Verma, R.; Muqet, M.A. High speed integrated RF–VLC data communication system: Performance constraints and capacity considerations. *Phys. Commun.* **2022**, *50*, 101492. [[CrossRef](#)]
30. Mayet, A.; Smith, C.E.; Hussain, M.M. Energy Reversible Switching from Amorphous Metal Based Nanoelectromechanical Switch. In Proceedings of the 13th IEEE International Conference on Nanotechnology (IEEE-NANO 2013), Beijing, China, 5–8 August 2013; pp. 366–369.
31. Khaibullina, K. Technology to Remove Asphaltene, Resin and Paraffin Deposits in Wells Using Organic Solvents. In Proceedings of the SPE Annual Technical Conference and Exhibition 2016, Dubai, United Arab Emirates, 26–28 September 2016.
32. Tikhomirova, E.A.; Sagirova, L.R.; Khaibullina, K.S. A review on methods of oil saturation modelling using IRAP RMS. *IOP Conf. Ser. Earth Environ. Sci.* **2019**, *378*, 012075. [[CrossRef](#)]
33. Khaibullina, K.S.; Korobov, G.Y.; Lekomtsev, A.V. Development of an asphalt-resin-paraffin deposits inhibitor and substantiation of the technological parameters of its injection into the bottom-hole formation zone. *Period. Tehe Quim.* **2020**, *17*, 769–781.
34. Khaibullina, K.S.; Sagirova, L.R.; Sandyga, M.S. Substantiation and selection of an inhibitor for preventing the formation of asphalt-resin-paraffin deposits. *Period. Tehe Quim.* **2020**, *17*, 541–551.
35. Mayet, A.M.; Alizadeh, S.M.; Kakarash, Z.A.; Al-Qahtani, A.A.; Alanazi, A.K.; Alhashimi, H.H.; Eftekhari-Zadeh, E.; Nazemi, E. Introducing a Precise System for Determining Volume Percentages Independent of Scale Thickness and Type of Flow Regime. *Mathematics* **2022**, *10*, 1770. [[CrossRef](#)]

36. Mayet, A.M.; Alizadeh, S.M.; Nurgalieva, K.S.; Hanus, R.; Nazemi, E.; Narozhnyy, I.M. Extraction of Time-Domain Characteristics and Selection of Effective Features Using Correlation Analysis to Increase the Accuracy of Petroleum Fluid Monitoring Systems. *Energies* **2022**, *15*, 1986. [[CrossRef](#)]
37. Hanus, R.; Zych, M.; Golijanek-Jędrzejczyk, A. Investigation of Liquid–Gas Flow in a Horizontal Pipeline Using Gamma-Ray Technique and Modified Cross-Correlation. *Energies* **2022**, *15*, 5848. [[CrossRef](#)]
38. Hosseini, S.; Roshani, G.H.; Setayeshi, S. Precise gamma based two-phase flow meter using frequency feature extraction and only one detector. *Flow Meas. Instrum.* **2020**, *72*, 101693. [[CrossRef](#)]
39. Roshani, M.; Ali, P.J.; Roshani, G.H.; Nazemi, B.; Corniani, E.; Phan, N.H.; Tran, H.N.; Nazemi, E. X-ray tube with artificial neural network model as a promising alternative for radioisotope source in radiation based two phase flowmeters. *Appl. Radiat. Isot.* **2020**, *164*, 109255. [[CrossRef](#)]
40. Peyvandi, R.G.; Rad, S.I. Application of artificial neural networks for the prediction of volume fraction using spectra of gamma rays backscattered by three-phase flows. *Eur. Phys. J. Plus* **2017**, *132*, 511. [[CrossRef](#)]
41. Roshani Gholam, H.; Ehsan, N.; Farzin, S.; Mohammad, A.I.; Salar, M. Designing a simple radiometric system to predict void fraction percentage independent of flow pattern using radial basis function. *Metrol. Meas. Syst.* **2018**, *25*, 347–358.
42. Roshani, G.H.; Nazemi, E.; Feghhi, S.A.H.; Setayeshi, S. Flow regime identification and void fraction prediction in two-phase flows based on gamma ray attenuation. *Measurement* **2015**, *62*, 25–32. [[CrossRef](#)]